Theoretical analysis of temperature sensor based on dual-core fiber

Daru Chen (陈达如)[1,2*], Gufeng Hu (胡顾锋)[1], Baojin Peng (彭保进)[1], Genzhu Wu (吴根柱)[1], and H. Y. Tam (谭华耀)[2]

[1]*Institute of Information Optics, Zhejiang Normal University, Jinhua 321004, China*

[2]*Photonics Research Centre, Department of Electrical Engineering, The Hong Kong Polytechnic University, Hong Kong SAR, China*

[*]*Corresponding author: daru@zjnu.cn*

Received August 10, 2011; accepted October 25, 2011; posted online April 18, 2012

A novel temperature sensor based on a dual-core fiber (DCF) is proposed and theoretically analyzed. The DCF-based temperature sensor is simply formed by splicing a segment of DCF to two segments of single mode fibers, where the DCF is used as the sensing element. The mode coupling between two fiber cores of the DCF is sensitive to the temperature-induced index change of the silica in the DCF. Simulations show that there is a linear relationship between the temperature of the DCF and the wavelength shift of the output spectrum of the DCF-based temperature sensor when the broadband light is injected into one fiber core of the DCF. Temperature sensors based on DCFs with different parameters for temperature sensing are also investigated.

OCIS codes: 060.2310, 060.2280, 060.2370.
doi: 10.3788/COL201210.S10601.

Optical fiber sensors have attracted considerable attention in the past three decades due to their advantages such as small size, light weight, high sensitivity, multiplexing capability, immunity to electromagnetic interference, and so on[1−5]. Among them, temperature sensors based on optical fiber devices using various techniques such as Raman and Brilllouin scattering[6−9], fiber Bragg grating (FBG)[10−12], long-period fiber grating (LPG)[13,14], and interferometry[15−18] have been extensively investigated due to their broad applications in fundamental research, electrical power engineering, astronautical engineering, energy and power engineering, and chemical industry. Temperature sensors based on the Raman/Brilllouin scattering have successfully achieved distributed temperature measurement but suffer from the limited measurement range (less than 100 °C). FBG and LPG are two of the most particular temperature fiber sensors because of its capability of multiplexing. However, we need costly fabrication system for the FBG (LPG) and the operational temperature of the FBG (LPG) fabricated using UV laser writing is usually very low (e.g., 300 °C for the FBG written into the B- and Ge-codoped silicate fiber) due to the poor thermal stability of the UV-induced refractive index change[19]. Special matericals or fabrication processing are needed for high-temperature FBG sensors[20−23]. Temperature sensors based on Fabry–Perot interferometer[24−26] and modal interferometer[27,28] have successfully achieved high-temperature sensing, among which special fibers such as the photonic crystal fiber and multimode fiber (MMF) have been used for high-temperature sensing.

In this letter, we propose a kind of novel temperature sensor based on a dual-core fiber (DCF) with an operational principle of the mode coupling between two fiber cores (formed two individual waveguides). The DCF-based temperature sensor is simply formed by splicing a segment of DCF to two segments of single mode fibers (SMFs). Temperature information is achieved by measuring the wavelength shift of the output spectrum of the DCF-based temperature sensor. The proposed DCF-based temperature sensor can be used for high temperature (> 1 000 °C) sensing with a sensitivity of about 7 pm/°C.

Figure 1(a) shows the cross-section of the proposed DCF. Two fiber cores (α and β) with the diameter (d) and the center-to-center distance (H) are arranged symmetrically in the cross-section of the DCF. The outside diameter of the DCF is D, which is fixed to be 125 μm to match the SMF. To simplify analysis, the refractive index of the silica under the reference temperature $T = 0$ °C is assumed to be 1.45 and the refractive index difference between the fiber core and fiber cladding is δ, which is 0.32%, 0.36%, and 0.40% for different DCFs in our calculations, respectively. Figure 1(b)

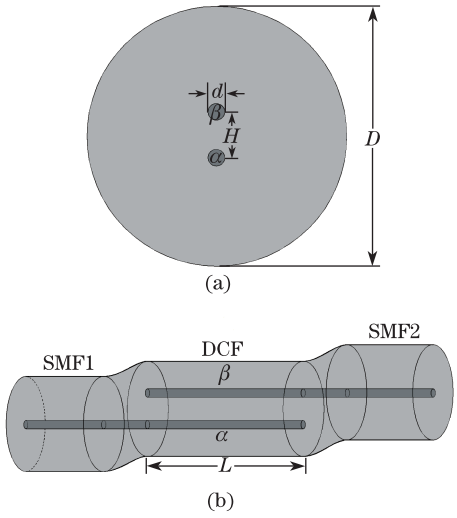

Fig. 1. (a) Cross-section of the proposed DCF and (b) structure of the DCF-based temperature sensor.

shows the structure of the temperature sensor based on the proposed DCF. A segment of the proposed DCF with a length (L) is spliced to SMF1 by matching fiber core α to the fiber core of SMF1 on one side and to SMF2 by matching fiber core β to the fiber core of SMF2 on another side, which results in an offset between the DCF and the SMF on both sides. The broadband light is injected to the fiber core α through SMF1 and we detect the signal on the output side of the fiber core β through SMF2.

The operational principle of the temperature sensor is based on the thermooptic effect and the mode coupling of the DCF. The thermooptic coefficient of the silica is $\mathrm{d}n/\mathrm{d}T = 10^{-5}/^{\circ}\mathrm{C}$[29], and we have the refractive index of the silica under the temperature (T)

$$n = 1.45 + T \times 10^{-5}, \tag{1}$$

which indicates the effective index of the DCF depends on the temperature (T). The mode coupling of the two fiber cores in the DCF is briefly introduced as follows. Suppose that the powers of the injected light on the input side of the fiber core α (SMF1) and the fiber core β are 1 and 0, respectively. According to the conventional coupled-mode theory[30], the output power on the output side of the fiber core α and the fiber core β (SMF2) of the DCF with a length (L) can be given by

$$P_1(L) = \cos^2(SL) + \cos^2(\eta)\sin^2(SL), \tag{2}$$

$$P_2(L) = \sin^2(\eta)\sin^2(SL), \tag{3}$$

where the later one is the output power of the DCF-based temperature sensor. Note that we have

$$\begin{aligned} &S = |n_{\mathrm{e}} - n_{\mathrm{o}}|\pi/\lambda, \\ &S = \sqrt{\delta^2 + \kappa^2}, \\ &\tan(\eta) = \kappa/\delta, \\ &\delta = |n_{\mathrm{a}} - n_{\mathrm{b}}|\pi/\lambda, \end{aligned} \tag{4}$$

where λ, $n_{\mathrm{e}}(n_{\mathrm{o}})$, and $n_{\mathrm{a}}(n_{\mathrm{b}})$ are the operational wavelength, the effective index of the even (odd) mode of two fiber cores, and the effective index of individual fiber core α (β). For the DCF, we have $\delta = 0$ since the fiber core α and the fiber core β are symmetrical in the DCF. Thus, Eqs. (2) and (3) can be rewritten as

$$P_1(L) = \cos^2(SL), \tag{5}$$

$$P_2(L) = \sin^2(SL). \tag{6}$$

Let $\Delta n_{\mathrm{eo}} = |n_{\mathrm{e}} - n_{\mathrm{o}}|$, which is dependent on both the operational wavelength and the temperature. Then the output power of the DCF-based temperature sensor is

$$P_2(T,\lambda) = \sin^2(|n_{\mathrm{e}} - n_{\mathrm{o}}|\pi L/\lambda) = \sin^2[\Delta n_{\mathrm{eo}}(T,\lambda)\pi L/\lambda], \tag{7}$$

where we can achieve temperature information by measure the output spectrum of the DCF-based temperature sensor due to $P_2(T,\lambda)$.

The proposed DCF has two basic modes with the effective index (n_{e}) for the even mode and the effective index (n_{o}) for the odd mode. A well-known finite-element method (FEM)[31] which can calculate the effective index and mode profile is used to investigate the guiding modes of the DCF. Figure 2 shows the normalized electric field distribution along the radial direction for the even mode and the odd mode of the DCF with parameters of $H = 12$ μm, $d = 8.2$ μm, and $\delta = 0.36\%$. The operational wavelength is λ=1 550 nm and the DCF is under the reference temperature $T = 0$ °C. Insets show the corresponding mode profiles of the electric field. By using the FEM, we can achieve the calculated effective indices which are $n_{\mathrm{e}} = 1.4523821258$ for the even mode and $n_{\mathrm{o}} = 1.4521005751$ for the odd mode of the DCF, which indicates the coupling length of two fiber cores is $L_{\mathrm{c}} = \pi/(2S)$=0.55 cm. Figure 3(a) shows the value (around 2.8×10^{-4}) of Δn_{eo} which varies very slowly in the wavelength range from 1 540 to 1 560 nm in the case of the reference temperature $T = 0$ °C. Regarding to a temperature sensor based on a DCF with a length of 10 cm (15 cm), when an ideal broadband optical source with uniform output power for each wavelength is used as the optical source of the DCF-based temperature sensor, we have the output spectrum shown as the solid (dotted) curve with a sine-function-like profile in Fig. 3(b) according to Eq. (7). This is the case for the DCF under the reference temperature $T = 0$ °C.

For the DCF under different temperatures, the FEM is used to calculate the effective indices of the even mode and the odd mode and different output spectra is achieved based on Eq. (7). Figure 4(a) shows the output spectra of the DCF-based temperature sensor when the 10-cm DCF is under temperatures 0, 200, 400, 600, 800, and 1 000 °C, respectively. We can find that the output spectrum shifts to the longer wavelength

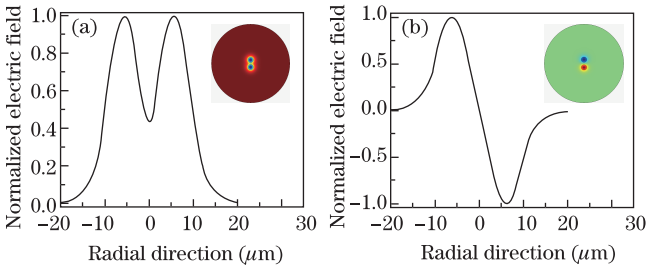

Fig. 2. Normalized electric field distribution along the radial direction for (a) the even mode and (b) the odd mode of the DCF with parameters of $H = 12$ μm, $d = 8.2$ μm, and $\delta = 0.36\%$. Insets show the corresponding mode profiles of the electric field.

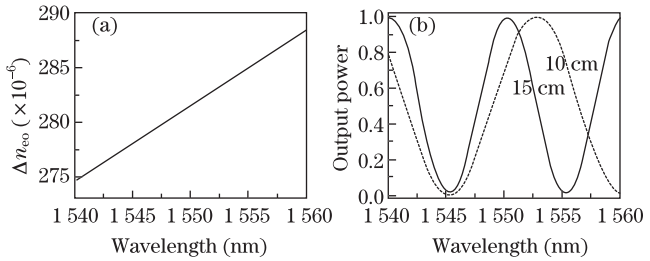

Fig. 3. (a) Δn_{eo} versus wavelength in the range from 1 540 to 1 560 nm and (b) output spectrum of the temperature sensor based on 10 cm (dotted curve) or 15 cm (solid curve) DCF.

when the temperature increases, which is due to the decreased value of $\Delta n_{\rm eo}$ for high temperature. The sensitivity of the DCF-based temperature sensor is about 0.0072 nm/°C. Figure 4(b) shows the valley wavelength (around 1 550 nm) of the output spectrum of the DCF-based temperature sensor for different temperatures. It can be seen that there is a linear relationship between the valley wavelength and the temperature.

Figure 5 shows the wavelength shift of the output spectrum of the temperature sensor based on DCFs with different parameters: (H = 12 μm, d = 8.2 μm, δ = 0.36%), (H = 13 μm, d = 8.2 μm, δ = 0.36%), (H = 11 μm, d = 8.2 μm, δ = 0.36%), (H = 12 μm, d = 9.0 μm, δ = 0.36%), (H = 12 μm, d = 7.4 μm, δ = 0.36%), (H = 12 μm, d = 8.2 μm, δ = 0.40%), and (H = 12 μm, d = 8.2 μm, δ = 0.32%). Note that all DCFs have the same length of 10 cm. Inset of Fig. 5 shows a partial enlarged view for the temperature T = 1 000 °C, it can be seen that DCF can achieve larger wavelength shift for the same temperature. Considering the DCF with parameters of H = 12 μm, d = 8.2 μm, and δ = 0.36% as a reference, we can conclude that smaller H, larger d, or smaller δ of the DCF will result in larger wavelength shift for the same temperature increment. In other words, stronger mode coupling of two fiber cores in the DCF will result in higher sensitivity of the DCF-based temperature sensor.

In conclusion, we propose and numerically investigate a temperature sensor based on DCF. Our calculations show that the proposed DCF can be used as a temperature sensing element based on the thermooptic effect and the mode coupling of the two fiber cores. The performance of the DCF-based temperature sensor is theoretically analyzed. The linear relationship between the temperature of the DCF and the wavelength shift of the output spectrum is presented. Temperature sensors based on DCFs with different structure parameters are discussed.

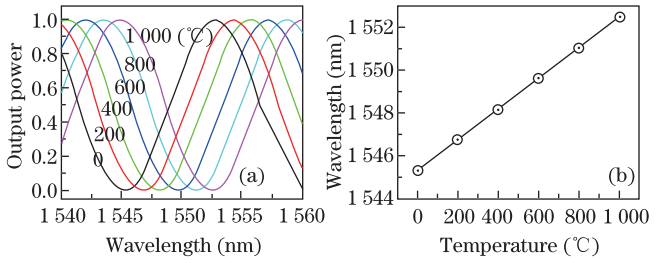

Fig. 4. (a) Output spectra of the DCF-based temperature sensor when the DCF is under temperature of 0, 200, 400, 600, 800, and 1 000 °C, respectively. (b) Valley wavelengths around 1 550 nm of the output spectra of the DCF-based temperature sensor for different wavelengths.

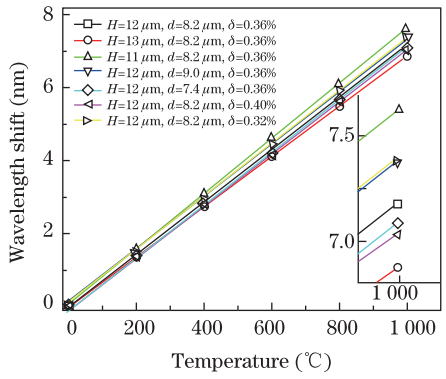

Fig. 5. Wavelength shift of the output spectrum of temperature sensors based on DCFs with different parameters.

This work was supported partially by the National Natural Science Foundation of China (No. 61007029), the Projects of Zhejiang Province (Nos. 2011C21038 and 2010R50007), and the Central Research Grant of The Hong Kong Polytechnic University under the Postdoctoral Fellowship (No. G-YX2D).

References

1. G. Gagliardi, M. Salza, P. Ferraro, and P. De Natale, Opt. Express **13,** 2377 (2005).
2. S. Konorov, A. Zheltikov, and M. Scalora, Opt. Express **13,** 3454 (2005).
3. M. Niklès, L. Thévenaz, and P. A. Robert, Opt. Lett. **21,** 758 (1996).
4. A. D. Kersey, M. A. Davis, H. J. Patrick, M. LeBlanc, K. P. Koo, C. G. Ashins, M. A. Putnam, and E. J. Friebele, J. Lightwave Technol. **15,** 1442 (1997).
5. B. Culshaw, J. Lightwave Technol. **22,** 39 (2004).
6. J. P. Dakin, D. J. Pratt, G. W. Bibby, and J. N. Ross, Electron. Lett. **21,** 569 (1985).
7. M. A. Farahani and T. Gogolla, J. Lightwave Technol. **17,** 1379 (1999).
8. T. Kurashima, T. Horiguchi, and M. Tateda, Opt. Lett. **15,** 1038 (1990).
9. X. Bao, M. DeMerchant, A. Brown, and T. Bremner, J. Lightwave Technol. **19,** 1698 (2001).
10. K. O. Hill and G. Meltz, J. Lightwave Technol. **5,** 1263 (1997).
11. B.-O. Guan, H.-Y. Tam, X.-M. Tao, and X.-Y. Dong, IEEE Photon. Technol. Lett. **12,** 675 (2000).
12. X. Shu, B. A. L. Gwandu, Y. Liu, L. Zhang, and I. Bennion, Opt. Lett. **26,** 774 (2001).
13. Y.-G. Han, S. Lee, C.-S. Kim, J. Kang, Y. Chung, and U.-C. Paek, Opt. Express **11,** 476 (2003).
14. K. J. Han, Y. W. Lee, J. Kwon, S. Roh, J. Jung, and B. Lee, IEEE Photon. Technol. Lett. **12**, 2114 (2004).
15. P. A. Leilabady and M. Corke, Opt. Lett. **12**, 772 (1987).
16. H.-S. Choi and H. F. Taylor, Opt. Lett. **22**, 1814 (1997).
17. Z. Tian and S. S.-H. Yam, J. Lightwave Technol. **27,** 2296 (2009).
18. C. R. Liao, Y. Wang, D. N. Wang, and M. W. Yang, IEEE Photon. Technol. Lett. **22,** 1686 (2010).
19. Y. Shen, J. He, Y. Qiu, W. Zhao, S. Chen, T. Sun, and K. T. V. Grattan, J. Opt. Soc. Am. B **24,** 430 (2007).
20. Y. Zhu, P. Shum, H. Bay, M. Yan, X. Yu, J. Hu, J. Hao, and C. Lu, Opt. Lett. **30,** 367 (2005).
21. Y. Zhu, Z. Huang, F. Shen, and A. Wang, Opt. Lett. **30,** 711 (2005).
22. S. Bandyopadhyay, J. Canning, M. Stevenson, and K. Cook, Opt. Lett. **33,** 1917 (2008).
23. S. J. Mihailov, D. Grobnic, and C. W. Smelser, Opt. Lett. **35,** 2810 (2010).
24. H. Y. Choi, K. S. Park, S. J. Park, U.-C. Paek, B. H. Lee, and E. S. Choi, Opt. Lett. **33,** 2455 (2008).
25. Y.-J. Rao, M. Deng, T. Zhu, and H. Li, J. Lightwave

Technol. **27,** 4360 (2009).

26. C. Wu, H. Y. Fu, K. K. Qureshi, B.-O. Guan, and H. Y. Tam, Opt. Lett. **36,** 412 (2011).
27. S. H. Aref, R. Amezcua-Correa, J. P. Carvalho, O. Frazao, P. caldas, J. L. Santos, F. M. Araujo, H. Latifi, F. Farahi, L. A. Ferreira, and J. C. Knight, Opt. Express **17,** 18669 (2009).
28. Y. Geng, X. Li, X. Tan, Y. Deng, and Y. Yu, Appl. Opt. **50,** 468 (2011).
29. T. Martynkien, G. Statkiewicz-Barabach, J. Olszewski, J. Wojcik, P. Mergo, T. Geernaert, C. Sonnenfeld, A. Anuszkiewicz, M. K. Szczurowski, K. Tarnowski, M. Makara, K. Skorupski, J. Klimek, K. Poturaj, W. Urbanczyk, T. Nasilowski, F. Berghmans, and H. Thienpont, Opt. Express **18,** 15113 (2010).
30. W. P. Huang, J. Opt. Soc. Am. A **11,** 963 (1994).
31. K. Saitoh and M. Koshiba, IEEE J. Quantum Electron. **38,** 927 (2002).